energies

MDPI

Article

Development of Machine Learning-Based Production Forecasting for Offshore Gas Fields Using a Dynamic Material Balance Equation

Junhyeok Hyoung [1], Youngsoo Lee [2,3] and Sunlee Han [3,*]

[1] Department of Digital Social Innovation, Institute for Information & Communication Technology Planning & Evaluation, Daejeon 34054, Republic of Korea; hjh@iitp.kr
[2] Department of Environment and Energy, Jeonbuk National University, Jeonju 54896, Republic of Korea; youngsoo.lee@jbnu.ac.kr
[3] Department of Mineral Resource and Energy Engineering, Jeonbuk National University, Jeonju 54896, Republic of Korea
* Correspondence: slhan@jbnu.ac.kr; Tel.: +82-63-270-2358

Abstract: Offshore oil and gas fields pose significant challenges due to their lower accessibility compared to onshore fields. To enhance operational efficiency in these deep-sea environments, it is essential to design optimal fluid production conditions that ensure equipment durability and flow safety. This study aims to develop a smart operational solution that integrates data from three offshore gas fields with a dynamic material balance equation (DMBE) method. By combining the material balance equation and inflow performance relation (IPR), we establish a reservoir flow analysis model linked to an AI-trained production pipe and subsea pipeline flow analysis model. We simulate time-dependent changes in reservoir production capacity using DMBE and IPR. Additionally, we utilize SLB's PIPESIM software to create a vertical flow performance (VFP) table under various conditions. Machine learning techniques train this VFP table to analyze pipeline flow characteristics and parameter correlations, ultimately developing a model to predict bottomhole pressure (BHP) for specific production conditions. Our research employs three methods to select the deep learning model, ultimately opting for a multilayer perceptron (MLP) combined with regression. The trained model's predictions show an average error rate of within 1.5% when compared with existing commercial simulators, demonstrating high accuracy. This research is expected to enable efficient production management and risk forecasting for each well, thus increasing revenue, minimizing operational costs, and contributing to stable plant operations and predictive maintenance of equipment.

Keywords: offshore gas fields; machine learning; DMBE; production forecasting

Citation: Hyoung, J.; Lee, Y.; Han, S. Development of Machine Learning-Based Production Forecasting for Offshore Gas Fields Using a Dynamic Material Balance Equation. *Energies* **2024**, *17*, 5268. https://doi.org/10.3390/en17215268

Academic Editors: Hongfang Lu, Shanbi Peng, Enbin Liu and Weibiao Qiao

Received: 2 October 2024
Revised: 15 October 2024
Accepted: 21 October 2024
Published: 23 October 2024

1. Introduction

Globally, energy demand continues to rise steadily. According to the latest analysis by Statista, global natural gas consumption surged by 4.6% from 3832.1 billion cubic meter (BCM) in 2018 to 4010.2 BCM in 2023 [1]. This reflects a substantial increase of 18.9% compared with the 3372.1 BCM in 2013, indicating a significant upward trend. Concomitantly, interest in offshore oil and gas fields is growing alongside existing onshore production sites [2,3]. Unlike onshore facilities, which are relatively easier to maintain, production systems in subsea environments present complex challenges for maintenance and repair [4,5]. Therefore, designing optimal fluid production systems and operating real-time risk monitoring systems are crucial for ensuring the stability and safety of equipment.

In response to these challenges, smart operation technologies for gas fields, often referred to as digital oil field (DOF) technologies, are actively being developed [6]. These technologies leverage information and communications technology (ICT) to enhance production efficiency and safety by utilizing data collected from sensors attached to various

facilities [7,8]. Additionally, the oil and gas industry is increasingly exploring the application of machine learning based on big data, with AI techniques being employed for tasks such as fluid flow analysis in reservoirs and pipelines, production forecasting, and optimal network design [9,10]. The market research firm Markets and Markets predicts that the DOF industry will grow at an average annual rate of 6.3%, reaching approximately USD 43 billion by 2029 (Figure 1).

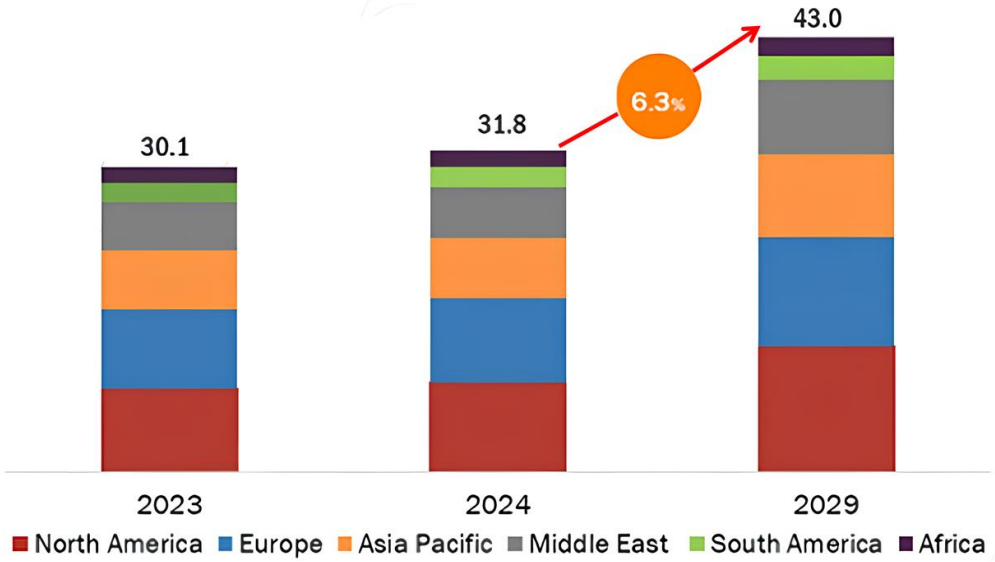

Figure 1. Digital oilfield market global forecast (USD billion) [11].

Petroleum development projects inherently face higher uncertainties than other resource development sectors, often leading to significant changes in initial development plans due to various challenges [12,13]. Gas fields are typically designed for production periods exceeding ten years, and alterations in development strategies can necessitate additional drilling and maintenance of both reservoirs and production facilities, ultimately impacting development and operational costs.

A recent study proposed a simplified analytical solution derived in real-time space, showing promising results in both onshore and offshore field cases [14]. However, such solutions often involve complex transformations and numerical inversions, which can introduce uncertainties. In the Volve Field case study in the North Sea, the Capacitance Resistance Model Injector Producer (CRMIP) model and automated seismic analysis were used to optimize well placement and predict production [15]. The complexity of these models can reduce interpretability, making it difficult to understand the underlying factors driving the predictions. Various prediction methods, such as acoustic emission, fiber optic sensing, infrared thermography, mass-volume balance, and pressure point analysis, have their own strengths and weaknesses. However, after evaluating key factors like accuracy, ease of use, and operational flexibility, dynamic modeling with machine learning stands out as the most effective [16]. Unlike mass-volume balance or pressure point analysis, which are limited to steady-state conditions, dynamic modeling adapts to both steady and transient states, offering superior accuracy and flexibility in real-time production environments [16–18].

To achieve successful gas field operations, it is essential to generate optimal development and maintenance plans through accurate analysis and diagnostics tailored to the target field [19]. Given the increasing complexity of offshore gas field management and the importance of accurate production forecasting, this study focuses on developing a machine learning-based solution to optimize production and ensure operational stability. A reservoir flow analysis model was developed using the dynamic material balance equation (DMBE), which integrates the mass balance method with the inflow performance relation (IPR). This model is further enhanced with an artificial intelligence (AI) component that

simulates production tubing and subsea pipeline flows. The integrated solution includes a rate allocation algorithm that predicts flow capacity for each production process and pipeline over time under normal operating conditions. This approach aims to establish a proactive maintenance solution capable of rapidly analyzing the flow characteristics of the entire production system. It is expected to enable quick calculations of production factors (such as pressure and temperature) for each production element, without relying on costly commercial software. Additionally, any abnormal signals generated during production can be swiftly identified, contributing to stable plant operations and proactive maintenance of equipment.

2. Theoretical Background and Method

2.1. Development of Analysis Method and the Change in Production Capacity of Reservoir

When production occurs through multiple wells, the reservoir pressure continuously declines [20]. The pressure drop pattern for each well varies due to the formation's heterogeneity and fluid properties, leading to changes in production capacity over time [21]. Variations in permeability and porosity of the reservoir cause uneven pressure depletion, gradually shifting the IPR curve downward as reservoir pressure decreases. Additionally, as gas composition changes or condensates form, the pressure-flow relationship adjusts, leading to further shifts in the IPR curve. This can be expressed through the IPR, which mathematically represents the relationship between reservoir pressure and flow rate and shows how the flow rate changes according to various flowing bottomhole pressures (FBHP) [22,23]. In gas fields, the IPR typically displays non-linear characteristics, as shown in Figure 2. Natural flow conditions can be determined at the intersection of the IPR and the tubing performance relationship (TPR) [24]. In Figure 2 it can be observed that the IPR curve shifts leftward and downward over time due to the reduction in reservoir pressure from production, explaining the decline in output over time as a shift in the intersection point.

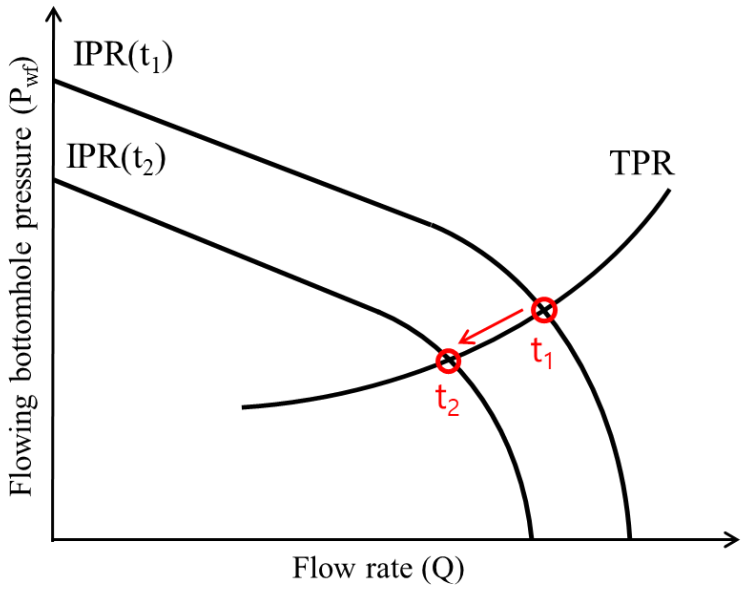

Figure 2. Time-dependent changes in inflow performance relationship (IPR) curves due to reservoir depletion.

In gas fields, simplified backpressure equations, such as Equation (1), are frequently used [25]. However, for more accurate analysis, more complex equations, like Equation (2), are preferred when pressures are comparable.

Backpressure equation:

$$q = C\left(P_R^2 - P_{wf}^2\right)^n \quad (1)$$

where, q = Gas flow rate (SCF/day), C = Performance coefficient (SCF/day/psi^2), P_R = Reservoir pressure (psia), P_{wf} = Flowing bottomhole pressure (psia) and n = exponent.

Compressible fluids under the pseudo steady-state flow condition:

$$Q_g = \frac{kh\left(P_R^2 - P_{wf}^2\right)}{1422T\left(\ln\frac{r_e}{r_w} - 0.75 + s\right)} \tag{2}$$

where, Q_g = Gas flow rate (MSCF/day), k = Permeability (md), T = temperature (°R), r_e = Drainage radius (ft), r_w = Wellbore radius (ft) and s = Skin factor.

For the analysis of the production flowline, pressure drops due to friction, gravitational effects, and other factors must be considered. For tubing, if either the FBHP or the wellhead pressure (WHP) is fixed, the pressure drop of fluid flowing through the tubing can be calculated using various charts or correlations, allowing the pressure at the other end to be determined [23]. The relationship between these flow pressures and flow rates is known as the TPR or flowline performance curve (FPC). A typical relationship for vertical flowlines is shown in Equation (3). The method follows the iterative approach described by Katz et al. [26], in which the compressibility factor is determined at the average pressure to ensure accurate pressure drop estimates.

Tubing performance relationship equation:

$$q = 200000\left[\frac{sD^5\left(P_{in}^2 - e^s P_{wh}^2\right)}{\gamma_g T z H f_M (e^s - 1)}\right]^{0.5} \tag{3}$$

where, D = Tubing diameter (inch), P_{in} = Flowing tubing intake pressure (psia), P_{wh} = Flowing wellhead pressure (psia), γ_g = Gas gravity temperature (°R), z = Average gas compressibility factor, H = Vertical depth (ft), $s = 0.0375\gamma_g$ H/Tz.

Moody friction factor:

$$f_M = \left[2\log\left(\frac{3.71}{\epsilon/D}\right)\right]^{-2} \tag{4}$$

where, ϵ = Absolute pipe roughness (in inches).

As previously mentioned, as production continues, the IPR curve shifts downward and to the left as reservoir pressure decreases, changing the intersection between the IPR and TPR over time. Since the IPR curve represents inflow-performance behavior at a specific point in time, linkage analysis with the material balance equation (MBE) is required to simulate the changing production capacity of oil wells over time [27]. The MBE treats the reservoir as a single tank and analyzes the average pressure, reserves, and productivity of the reservoir based on the conservation of mass for fluids entering and leaving the tank [28]. For gas fields, the MBE is a function of average reservoir pressure and cumulative gas production (Gp, SCF), and it incorporates the gas compressibility factor (z). This relationship is shown in Figure 3 and Equation (5), where it is represented as a linear function of p/z and Gp [29]. The average reservoir pressure can be derived from shut-in pressure recovery data during production stoppages.

MBE for gas reservoir:

$$\frac{P}{z} = \frac{P_i}{z_i} - \frac{G_P P_i}{G z_i} \tag{5}$$

where, P = Reservoir pressure (psia), P_i = Initial reservoir pressure (psia), z_i = Initial gas compressibility factor, G = Initial gas cap gas (SCF).

L. Mattar et al. have introduced a new concept called the flowing material balance equation (FMBE), which calculates initial gas in place (IGIP) using sandface flow pressure under constant production rates [29]. However, since most production wells do not maintain constant production rates over extended periods, the DMBE is applied. The DMBE can be expressed by the following Equations (6)–(9) [30].

Pseudo Steady-State Flow:

$$P_{in} - P_{wf} = \frac{qt}{c_o N} + b_{pss} q \quad (6)$$

Cumulative Production:

$$qt = N_P \quad (7)$$

MBE:

$$P_i - \overline{P_R} = \frac{N_P}{c_o N} \quad (8)$$

Combine Equations (6)–(8), and re-arrange:

$$\overline{P_R} = P_{wf} + b_{pss} q \quad (9)$$

This relationship shows how varying production pressures affect the IPR. Over time, the total production (N_P) increases, allowing p/z to be derived. Based on this derived p/z, the reservoir pressure can be recalculated, and by repeating this process, changes in the production capacity of the well over time can be predicted.

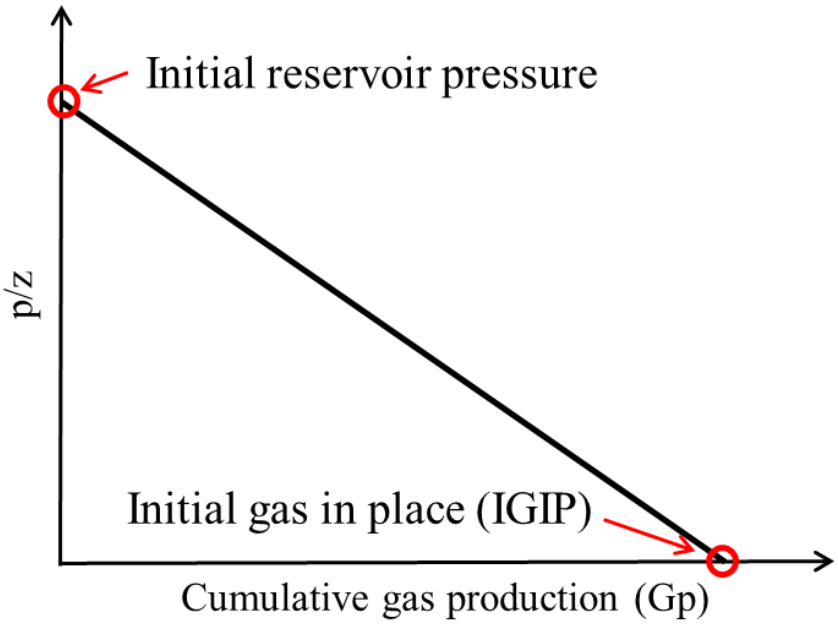

Figure 3. Material balance equation (MBE) plot for gas reservoir.

2.2. Development of In-Pipe Flow Prediction Model Using Artificial Intelligence

Artificial Neural Networks (ANNs) simulate the brain's network of neurons to create models, with deep learning specifically referring to ANNs that employ multiple layers [31]. For effective deep learning, large amounts of high-quality data are essential to create more accurate AI algorithms [32]. In recent years, machine learning techniques have been increasingly applied across various industries [33]. This study focused on predicting flow characteristics in production pipelines using a vertical flow performance (VFP) table, which represents the relationships among tubing head pressure (THP), water-gas ratio (WGR), oil-gas ratio (OGR), bottomhole pressure (BHP), and flow rate (Q). The goal was to develop an analysis method capable of predicting abnormalities that deviate from normal operating conditions by examining the correlations among THP, WGR, OGR, Q, and BHP.

Machine learning in this study was performed using TensorFlow 1.12.0, a Python-based library developed by Google [34,35]. The learning process proceeded as follows: first, parameter ranges were selected for each well and pipeline, resulting in an average of 80,000 datasets per flowline. Various techniques were then examined to identify the optimal

AI learning approach for training on the VFP tables. Recurrent neural networks (RNNs) were excluded from this study since the data points were independent and non-sequential. Instead, the study compared the learning accuracy of three methods: Multilayer perceptron (MLP) + Regression, Autoencoder + Regression, and Support vector regression (SVR). The variables used for each method, such as flow rate, pressure, and other operational conditions, and the structure of the neural networks are shown in Figures 4–6.

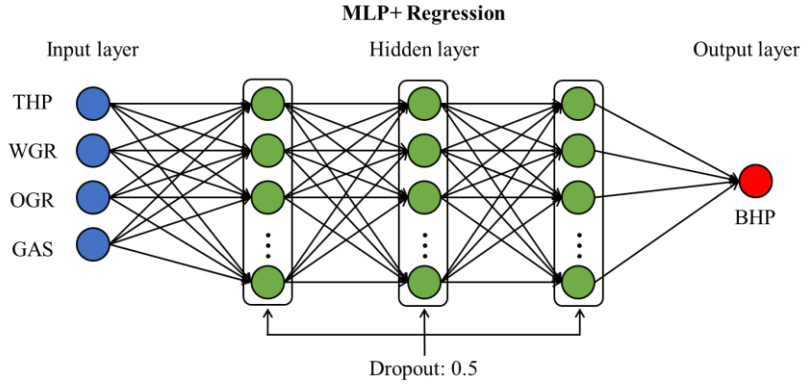

Input	4
Output	1
Batch size	Changeable
Epoch	8000
First hidden nodes	Changeable
Second hidden nodes	Changeable
Third hidden nodes	Changeable
Optimizing algorithm	Adam optimizer
Activation function	Leaky RELU/ tanh
Cost function	Mean square error (MSE)

Figure 4. Neural network structure and parameters for multilayer perceptron (MLP) + regression method.

The total learning dataset for each flowline was split into 75% for training, 15% for validation, and 10% for testing. To address variations in input data size and speed up the optimization process, data normalization was performed using a range from −1 to 1, as shown in Equation (10).

$$\text{Normalization} = 2 \times \frac{input - min}{max - min} - 1 \quad (10)$$

The model evaluation method confirmed that the predicted values fell within a range of ±20 psi using root mean square error (RMSE) to measure the difference between the predicted and actual values. Additionally, to avoid overfitting, the order of batch data was shuffled with each learning iteration. This approach helped ensure that the model generalized well and did not memorize the training data.

MLP, which achieved the highest accuracy, is a neural network with one or more intermediate (hidden) layers between the input and output layers, as shown in Figure 7. MLPs are feedforward networks, in which connections run from the input layer through the hidden layers to the output layer, without feedback from the output layer to the input layer.

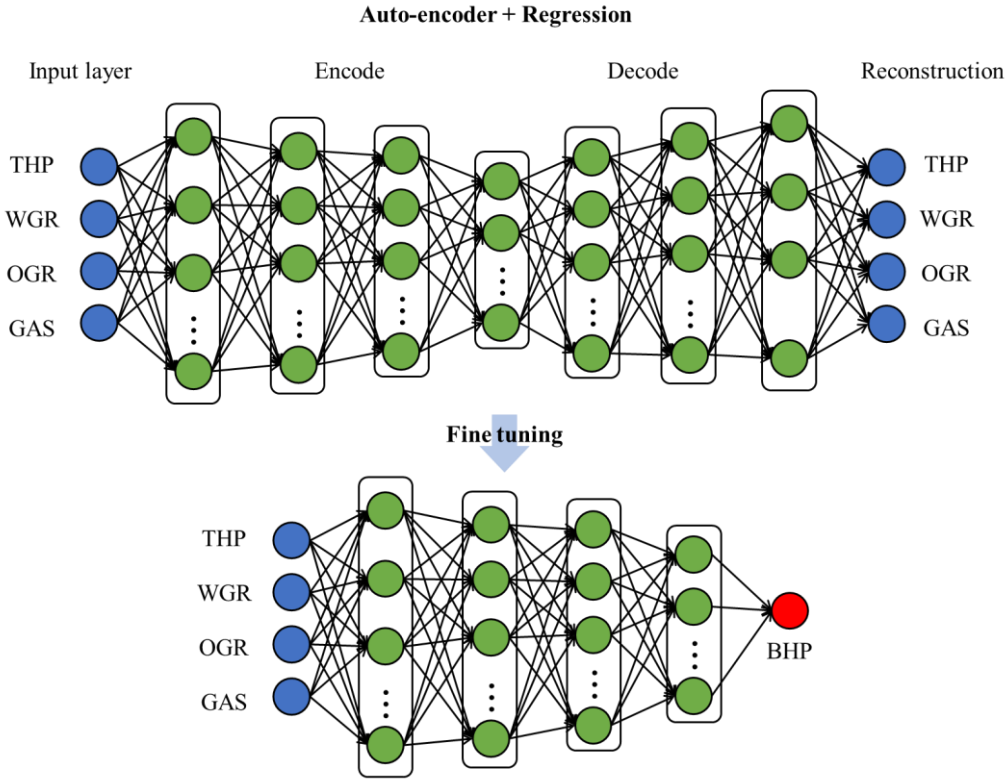

Input	4
Output	1
Batch size	Changeable
Auto-encoder epoch	8000
Fine tuning model epoch	8500
Hidden nodes	512, 256, 128, 64, 128, 256, 512
Optimizing algorithm	Adam optimizer
Activation function	Leaky RELU/ tanh
Cost function	Mean square error (MSE)

Figure 5. Neural network structure and parameters for auto-encoder + regression method.

Unlike a single-layer perceptron, MLP can analyze the nonlinear characteristics of input and output by utilizing these hidden layers, thereby improving predictive performance and overcoming the limitations of a single-layer perceptron. The accuracy of MLP or Autoencoder + Regression models generally depends on the number of hidden layers and nodes within those layers. Using the grid search method, we conducted repeated experiments to find the optimal number of hidden layers and nodes.

The performance of SVR, in contrast, depends on setting the appropriate hyperparameters, such as kernel type, gamma, penalty, and epsilon. In this study, SVR training on the VFP table was conducted by adjusting the remaining hyperparameters using the radial basis function (RBF). However, many overfitting issues arose, leading to suboptimal results. As a result, the MLP method was ultimately selected and used for AI training. This model selection process was vital in ensuring that the AI could handle the complexities of the data while maintaining high predictive accuracy, especially in dynamic production environments. The outcomes of each machine learning technique are presented in Tables 1–3.

Support vector regression (SVR)

$$y = \sum_{i=1}^{N}(a_i - a_i^*) \cdot K(x_i, x) + b \qquad K(x_i, x_j) = exp\left(-\frac{\|x_i - x_j\|^2}{2\sigma^2}\right)$$

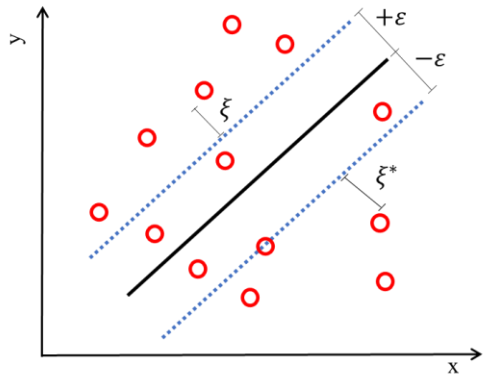

Input	4
Output	1
Learning data	Overall data-Validation data
Validation data	6240
Evaluation data	Overall data
γ	Changeable
ε	Changeable
Penalty constant	Changeable
Kernel (K)	RBF function
Evaluation function	Root mean square error (RMSE)

Figure 6. Structure and parameters for support vector regression (SVR) method. The asterisk (*) indicates the downward direction.

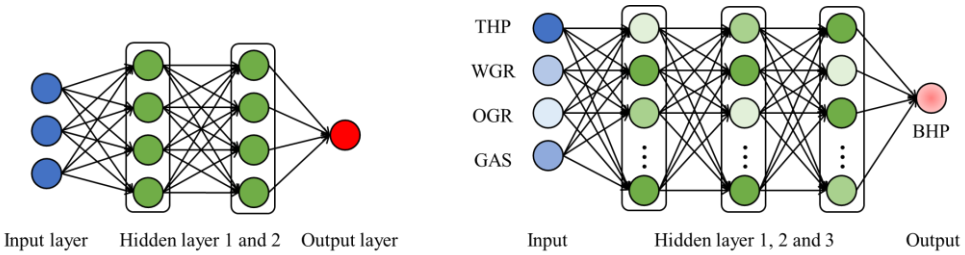

Figure 7. Optimized neural network structure for multilayer perceptron (MLP).

Table 1. Results of multilayer perceptron (MLP) model.

VFP Table Index	1st Hidden Node	2nd Hidden Node	3rd Hidden Node	Test Data	RMSE	±20 Range Count	±20 Range Count/ Total Data
1				6241	5.6952	6163	0.9876
2				6761	5.0745	6689	0.9893
3				7411	12.4004	6985	0.9425
4	512	1024	512	4941	6.9936	4786	0.9688
5				7001	10.8435	6677	0.9538
6				6751	11.4112	6445	0.9548
7				6881	4.9926	6812	0.9901

Table 2. Results of auto-encoder method.

VFP Table Index	1st Hidden Node	2nd Hidden Node	3rd Hidden Node	Test Data	RMSE	±20 Range Count	±20 Range Count/ Total Data
1	512	1024	512	6241	5.6952	6163	0.9876
2				6761	5.0745	6689	0.9893
3				7411	12.4004	6985	0.9425
4				4941	6.9936	4786	0.9688
5				7001	10.8435	6677	0.9538
6				6751	11.4112	6445	0.9548
7				6881	4.9926	6812	0.9901

Table 3. Results of support vector regression (SVR) method.

VFP Table Index	Kernel	Hyperparameters			Test Data	RMSE	±20 Range Count	±20 Range Count/ Total Data
		Gamma (γ)	Penalty (C)	Epsilon (ε)				
1	RBF	1	0.1	5×10^{-3}	6241	18.25427	1923	0.308124
		1	1	5×10^{-3}		16.73165	2098	0.336164
		1	10	5×10^{-3}		30.73826	1142	0.182983
		1	100	5×10^{-3}		16.33457	2149	0.344336
		10	0.1	5×10^{-3}		31.97001	1098	0.175933
		10	1	5×10^{-3}		29.62285	1185	0.189873
		10	10	1×10^{-3}		29.52318	1189	0.190514
		10	100	5×10^{-3}		15.98496	2196	0.351867
		100	0.1	5×10^{-3}		26.63355	1318	0.211184
		100	1	5×10^{-3}		30.26115	1160	0.185868
		100	10	5×10^{-3}		16.10967	2179	0.349143
		100	1000	5×10^{-3}		15.98496	2196	0.351867
		5	10	2×10^{-4}		30.36587	1156	0.185227
		8	10	2×10^{-4}		29.54800	1188	0.190354

As shown in the Tables 1–3, the goal was to predict the VFP table and BHP under specific flow conditions using the trained models. A predicted value within 20 psi of the actual value was considered a successful result. Both the MLP and Autoencoder methods achieved high prediction accuracy rates of nearly 97%. However, learning was less effective at the lower ends of the input values across all four variables. Through this process, it was demonstrated that machine learning models can predict pipeline flow characteristics with high accuracy, rivaling the results of existing pipeline flow simulators.

2.3. Building a Gas Field Optimal Operating Solution Using Rate Allocation Algorithm

Due to the reservoir's heterogeneity and fluid characteristics, the flow behavior of individual production flowlines can vary, even within the same gas field [25]. Therefore, applying rate allocation techniques is essential for accurately analyzing production across various flowlines. While gas production is influenced by several factors, the primary factor affecting flow rates—assuming reservoir and fluid properties remain constant—is the pressure at the top of the manifold [22]. When reservoir pressure is high, an adjustment at the manifold is applied to control the production rate [36]. In such cases, factors such as tubing depth, gas specific gravity, and pressure loss due to friction must be considered when gas flows through vertical production lines [37].

As production continues, reservoir pressures and other properties evolve, making it crucial to integrate and analyze the characteristics of each production system component to maintain optimal production conditions. This is especially important in manifolds where multiple wells and pipelines form a network. When extracting gas, production control must account for both economic factors and the reservoir's operational conditions. The production rate is largely determined by the pressure differential between upstream and

downstream points [38]. Since managing reservoir pressures poses economic and technical challenges, the common approach is to regulate pressure at the manifold.

In this study, we developed a production forecasting model for the entire production system by combining flow prediction models which were trained using IPR, DMBE, and machine learning techniques with yield distribution methods. The flowchart for this process is shown in Figure 8.

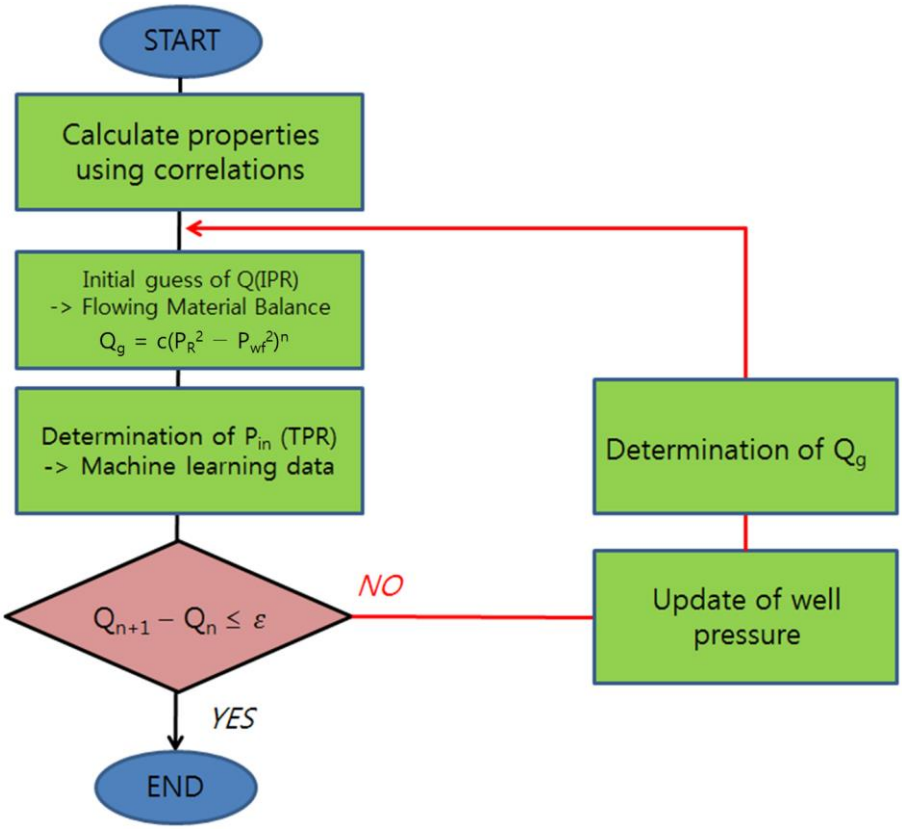

Figure 8. Flowchart of the rate allocation algorithm.

The model was designed to regulate the production rate of each well by calculating the necessary physical properties, simulating the IPR changes as production continues, and incorporating fluid material balance. Machine learning data was used to replace the TPR for more accurate predictions.

3. Results and Discussion

3.1. Model Accuracy

The accuracy of the machine learning model was assessed by comparing the predicted flow rates and BHP against values obtained from the commercial Pipesim™ (https://www.software.slb.com/software-news/software-top-news/pipesim/pipesim-2017-1 accessed on 3 September 2018) steady-state multiphase flow simulator. The properties of the gas wells used for simulating each field are detailed in Table 4.

Table 4. Key reservoir and wellbore characteristics for simulated offshore gas wells.

Well	Reservoir Pressure (psi)	C (Backpressure Eqn.)	n (Backpressure Eqn.)	Reservoir Temperature (°F)	Reservoir Depth (ft)
A	5293	2.216×10^{-5}	1	165.50	14,633
B	4800	3.106×10^{-5}	1	165.00	12,253
C	5200	1.857×10^{-5}	1	165.56	10,565

A virtual system was constructed using this model, which consisted of three gas wells, pipelines, chokes, and a manifold that gathers the gas produced and sends it to the platform, as illustrated in Figure 9. Well JUMPER (a pipeline) is a very short section, assumed to have minimal impact on the overall production process. Artificial intelligence learning data was generated for the production lines of wells A, B, and C, as well as for the pipelines running from the manifold to the platform. The gas fields used in this study are currently producing gas from three wells connected to a single manifold. Steady-state flow rates, BHP, THP, WGR, and OGR for each well were measured over several years and these values were matched precisely using the PIPESIM model. Using this model, we generated data under various operating conditions, resulting in the creation of 80,000 datasets.

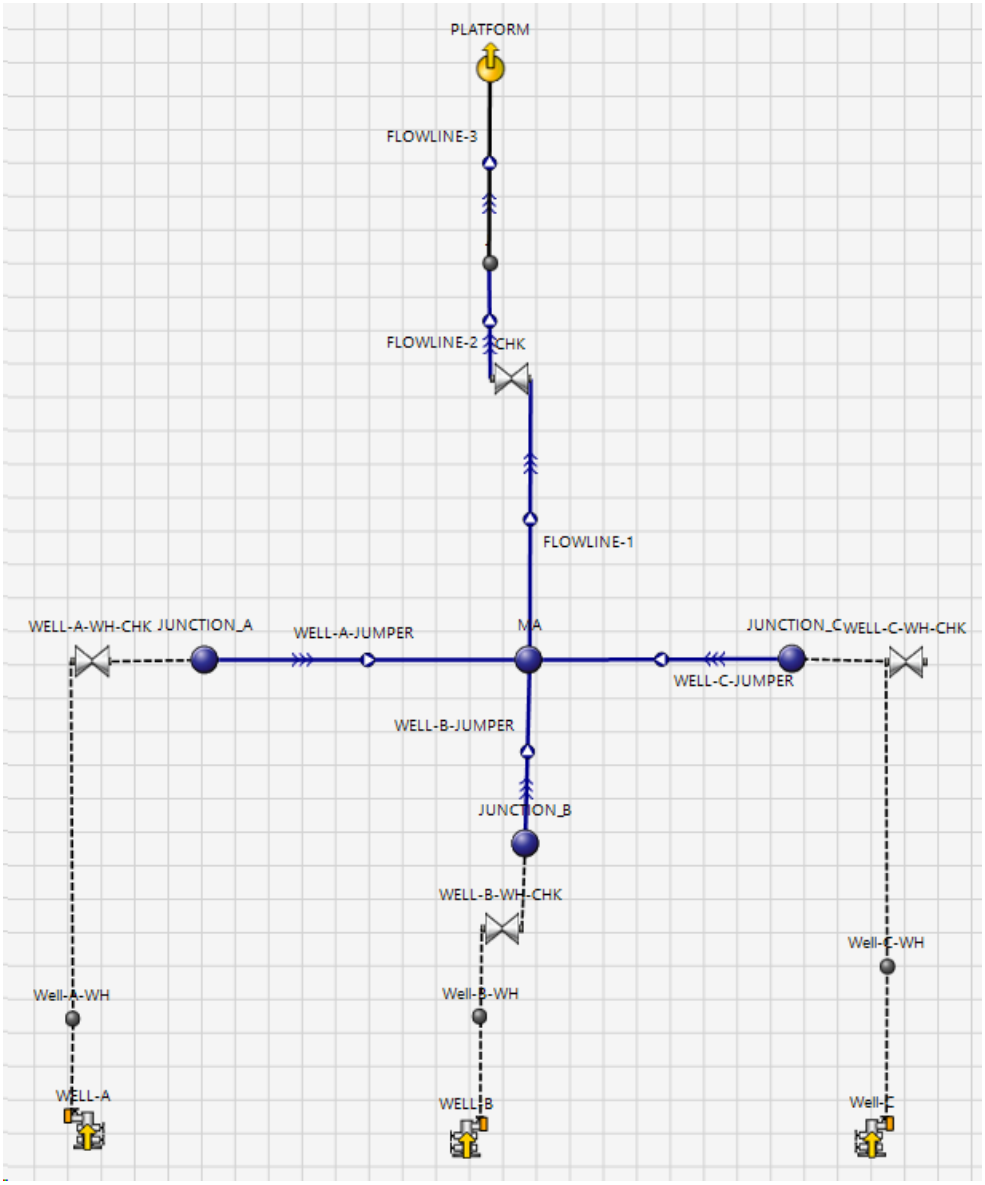

Figure 9. Schematic of PIPESIM simulation model for offshore gas wells and pipeline network.

In all three wells, the fluids produced were the same, with a very low water-cut, resulting in single-phase gas production. SLB's ECLIPSE software (https://www.software.slb.com/software-news/software-top-news/eclipse/eclipse-2017-1 accessed on 3 September 2018) was employed to calculate the mean reservoir pressure. Using the WBP9 (nine-block average) keyword, a 330-foot radius area was defined around each production well, and the average pressure for each area was calculated (see Figure 10).

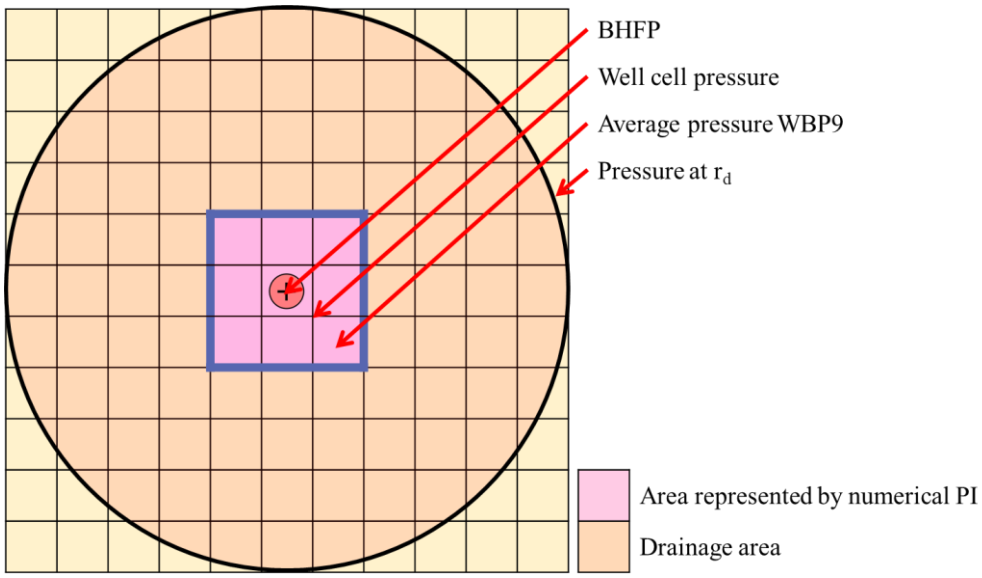

Figure 10. Application of the WBP9 (Nine-Block Average) method for pressure calculation.

Based on the simulation results, the material balance graphs for each gas well were plotted, along with the pressure-to-z relationship. These are shown in Figures 11–14. The resulting FMBE graph appears nearly linear. Given that the z-factor changes with pressure, an additional property calculation algorithm was included to reflect this variation. With FMBE, it is possible to calculate changes in reservoir pressure as a function of cumulative gas production. When combined with the IPR, this allows for changes in production capacity to be forecast while accounting for decreasing reservoir pressure.

Although most gas platforms are equipped with flowmeters for each well, several factors contribute to errors in the values measured [39]. Consequently, the exact production volume of each flowline is not always known, leading to operational challenges.

In this study, the previously described method and a Python script were used to develop a rate allocation algorithm capable of distributing the optimal output for each production process. By leveraging the machine learning data, the model was able to detect and respond to abnormal conditions in platform operations. The AI and algorithm-based system calculated the optimal output for each production process, verifying its accuracy by comparing the results with those from a commercial simulator.

Mean absolute error (MAE) was used to assess the model's accuracy. MAE is calculated from the mean of the absolute differences between predicted and actual values. It provides an intuitive measure of error and is commonly used to assess models for which minimizing the difference between predicted and actual values is critical. The closer the MAE value is to 0, the closer the predictions are to the actual values. The formula is as follows Equation (11):

$$MAE = \frac{1}{n}\sum|\hat{y} - y| \tag{11}$$

where, n = Number of points, $\hat{y}$ = Prediction value and y = True value.

The flow rate estimates for the three gas wells, based on specific cumulative production, are shown in Figures 15–18 and Tables 5–8 below.

Figure 15 and Table 5 show the comparison between simulated and estimated flow rates for Well A. As observed, the predicted flow rates closely match the simulated values, with only minor deviations across the production period. The trend line indicates that the flow rate steadily decreases from an initial rate of approximately 72 MMSCF/D to 58 MMSCF/D as cumulative gas production increases. This decline in flow rate is consistent with the reservoir depletion expected over time, which behavior the model captures accurately with minimal error.

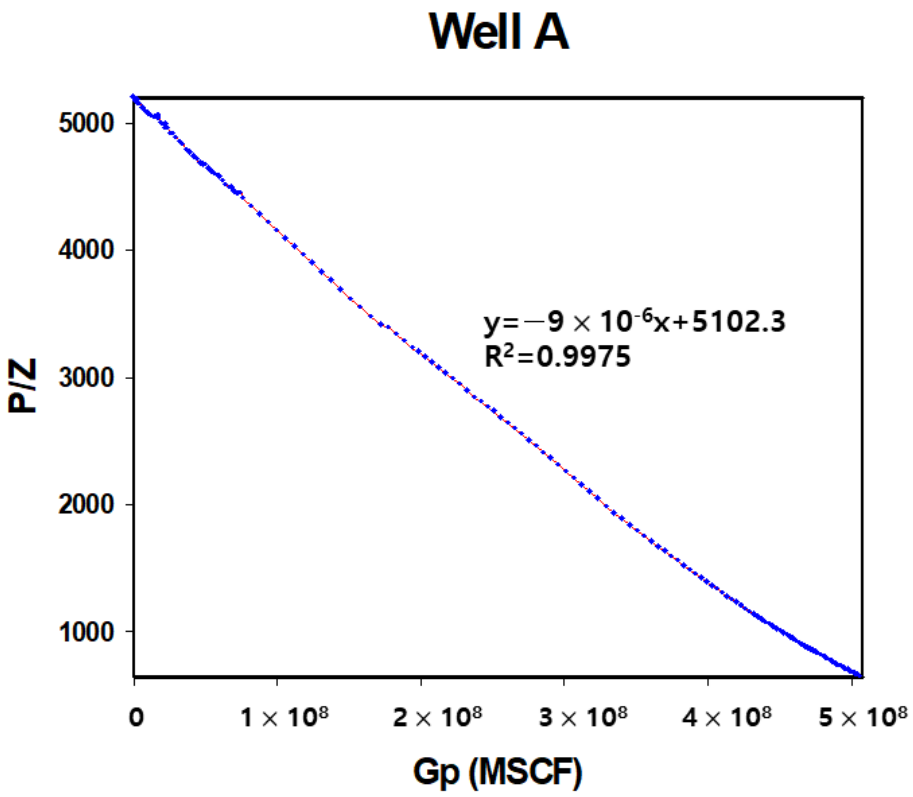

Figure 11. Material balance plot for Well A.

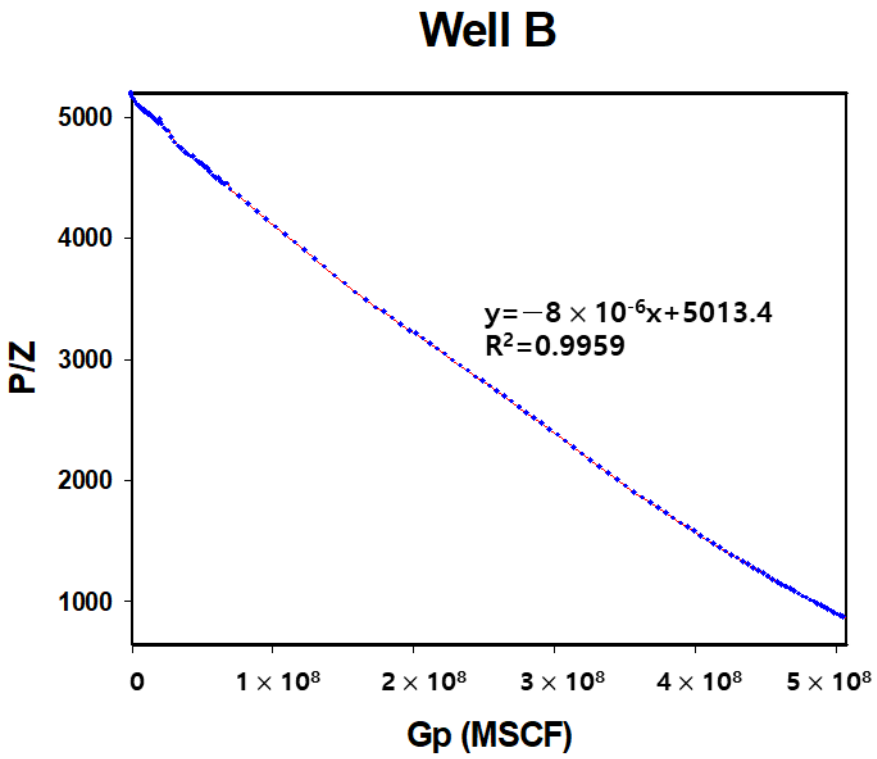

Figure 12. Material balance plot for Well B.

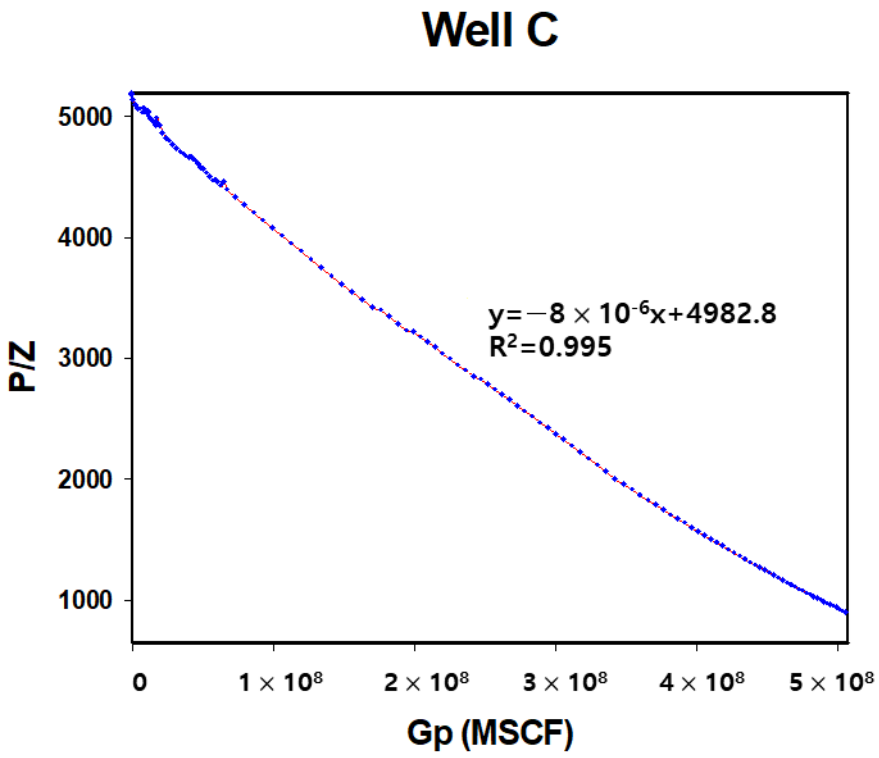

Figure 13. Material balance plot for Well C.

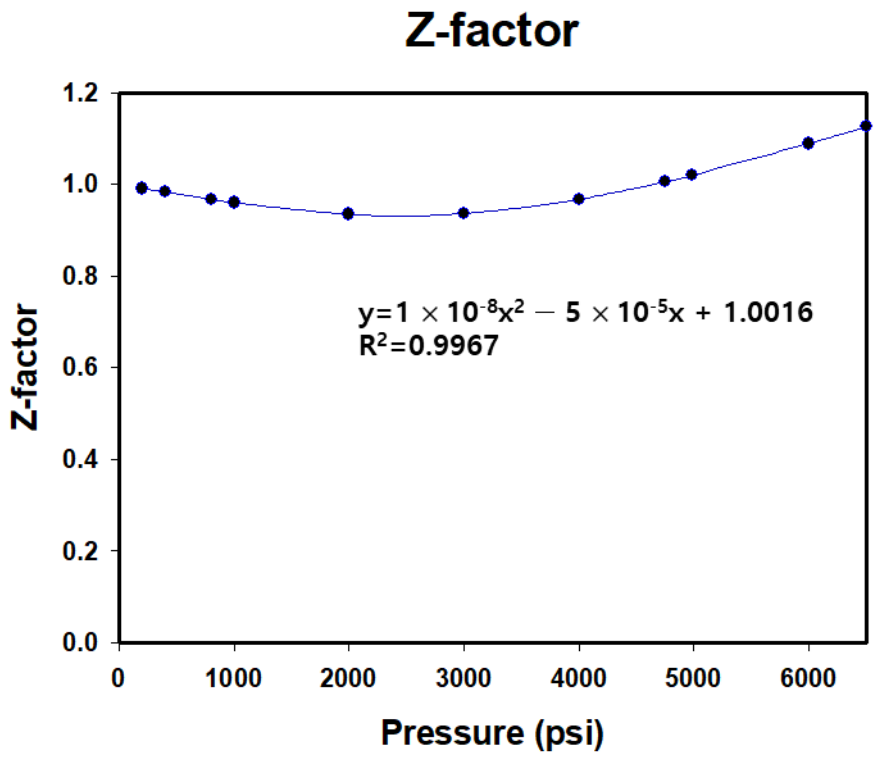

Figure 14. Gas compressibility (z-factor) variation with pressure in offshore gas reservoirs.

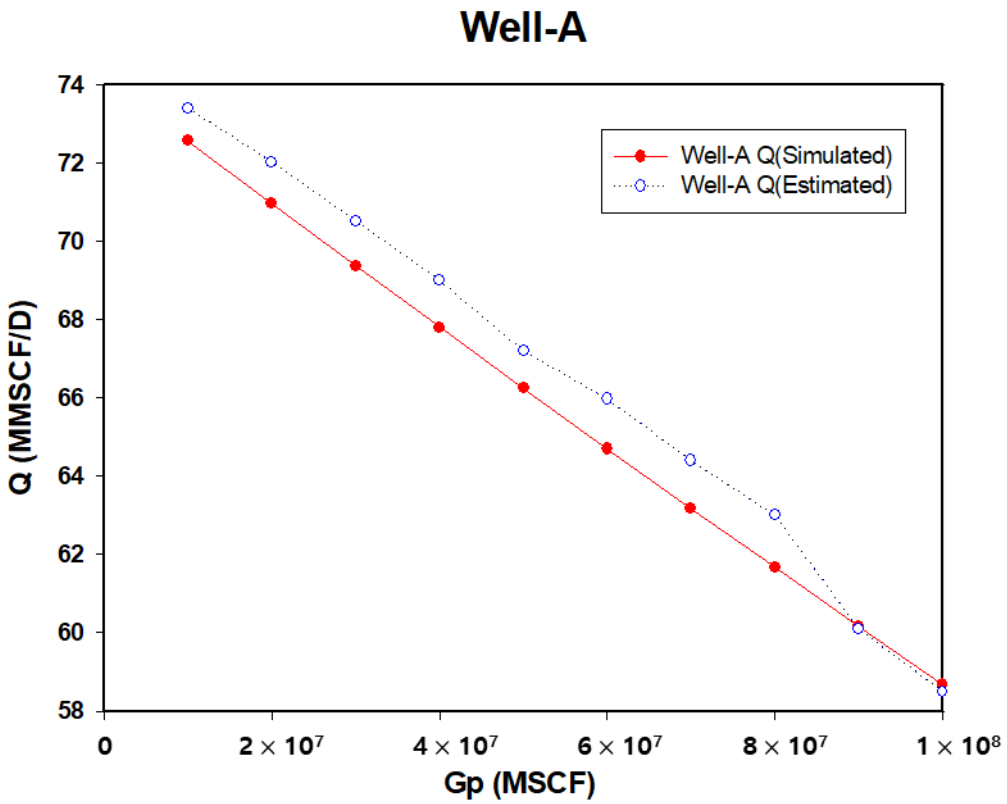

Figure 15. Simulated vs. Estimated flow rate for well A.

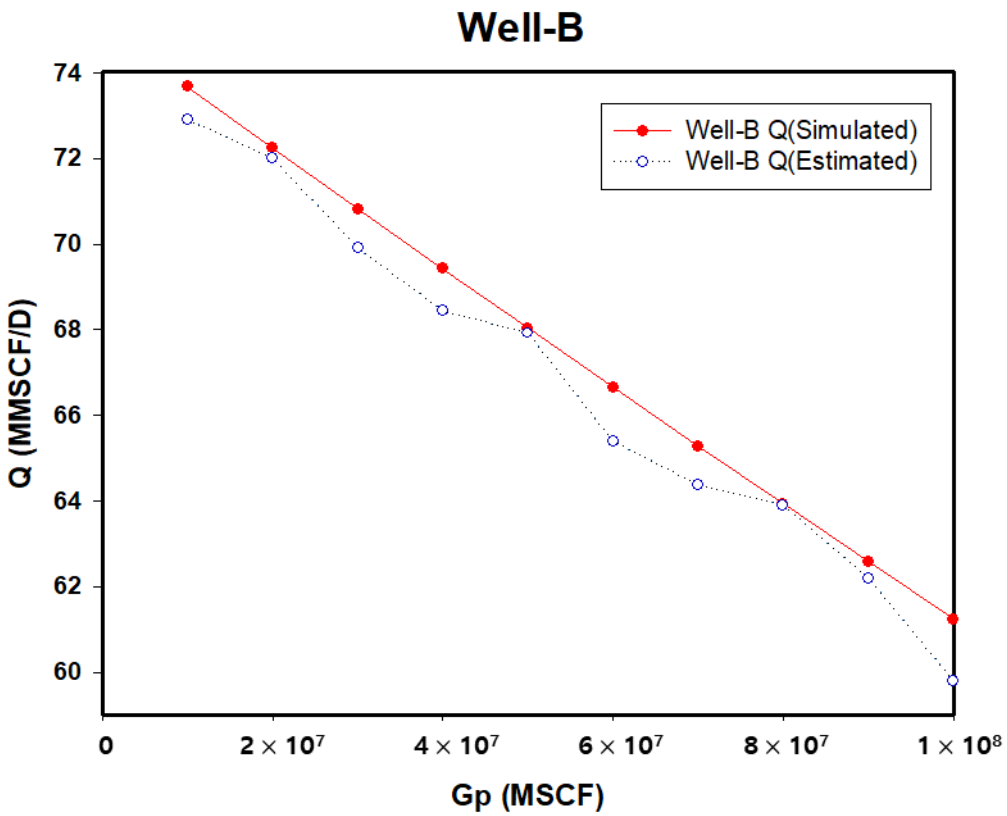

Figure 16. Simulated vs. Estimated flow rate for Well B.

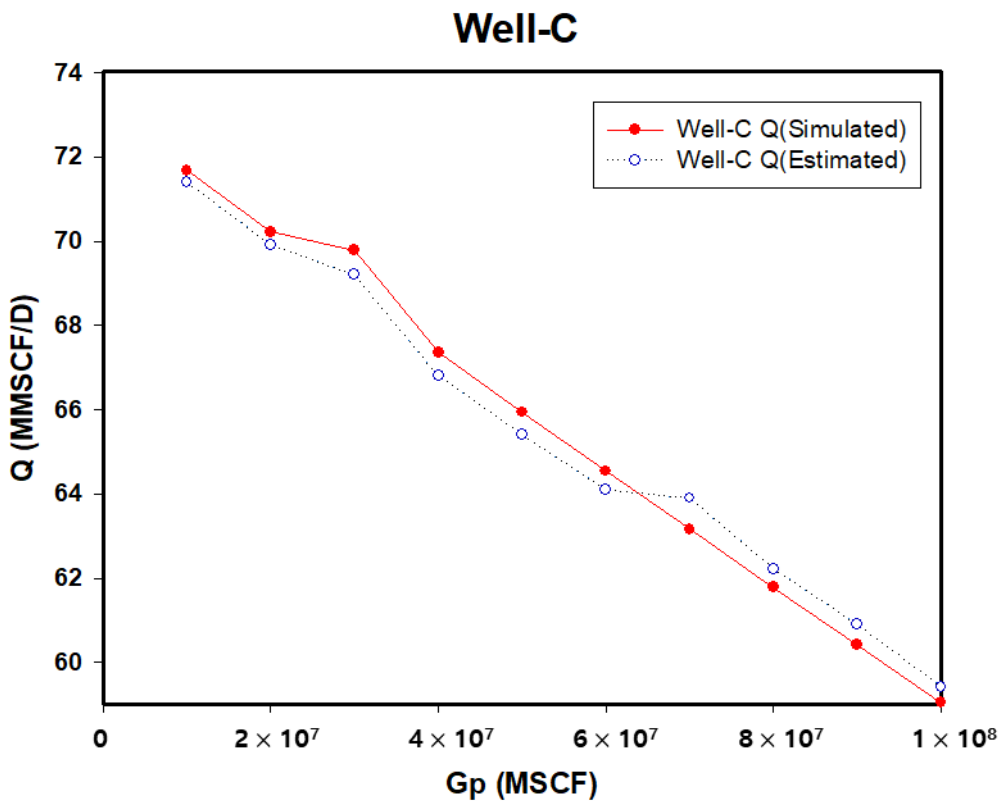

Figure 17. Simulated vs. Estimated flow rate for Well C.

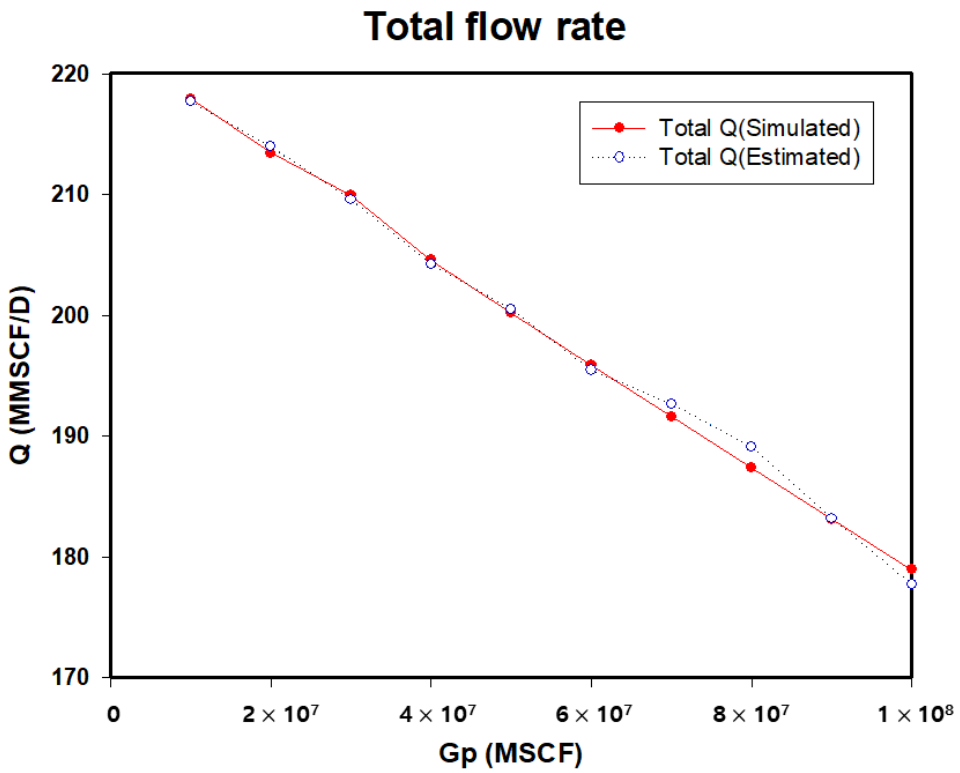

Figure 18. Simulated vs. Estimated total flow rate.

Table 5. Results of Well A: Simulated vs. Estimated production rates and bottomhole pressures.

Gp (MMSCF)	Well A Pressure (psi)	Well A Q (Simulated) (MMSCF/D)	Well A Q (Estimated) (MMSCF/D)	MAE
10,000	5149.83	72.57	73.40	0.9257
20,000	5027.16	70.96	72.03	
30,000	4907.93	69.37	70.51	
40,000	4791.82	67.80	69.00	
50,000	4678.57	66.24	67.20	
60,000	4567.92	64.70	65.97	
70,000	4459.66	63.17	64.40	
80,000	4353.59	61.67	63.00	
90,000	4249.55	60.16	60.10	
100,000	4147.38	58.67	58.50	

Table 6. Results of Well B: Simulated vs. Estimated production rates and bottomhole pressures.

Gp (MMSCF)	Well B Pressure (psi)	Well B Q (Simulated) (MMSCF/D)	Well B Q (Estimated) (MMSCF/D)	MAE
10,000	5028.64	73.67	72.90	0.702
20,000	4922.46	72.24	72.01	
30,000	4818.78	70.82	69.90	
40,000	4717.40	69.42	68.44	
50,000	4618.14	68.03	67.92	
60,000	4520.84	66.65	65.40	
70,000	4425.37	65.28	64.37	
80,000	4331.58	63.93	63.90	
90,000	4239.37	62.58	62.20	
100,000	4148.62	61.24	59.80	

Table 7. Results of Well C: Simulated vs. Estimated production rates and bottomhole pressures.

Gp (MMSCF)	Well C Pressure (psi)	Well C Q (Simulated) (MMSCF/D)	Well C Q (Estimated) (MMSCF/D)	MAE
10,000	4987.72	71.68	71.40	0.475
20,000	4882.52	70.22	69.91	
30,000	4779.74	69.78	69.20	
40,000	4679.19	67.36	66.80	
50,000	4580.70	65.94	65.40	
60,000	4484.12	64.54	64.10	
70,000	4389.30	63.16	63.90	
80,000	4296.13	61.78	62.22	
90,000	4204.49	60.41	60.90	
100,000	4114.27	59.05	59.42	

Similarly, Figure 16 and Table 6 present the comparison for Well B, for which the simulated and estimated flow rates also show a close correlation. In this case, the flow rate starts around 73 MMSCF/D and decreases to approximately 61 MMSCF/D over time. The accuracy of the model's predictions for Well B further confirms its robustness in handling varying reservoir conditions, with most deviations within an acceptable margin of error.

Figure 17 and Table 7 illustrate the same comparison for Well C, where the flow rate begins at 71 MMSCF/D and declines to around 59 MMSCF/D. The estimated values are almost identical to the simulated results, demonstrating the model's high precision in predicting the production performance of this well.

Table 8. Total simulated and estimated flow rates.

Gp (MMSCF)	Total Q (Simulated) (MMSCF/D)	Total Q (Estimated) (MMSCF/D)	MAE
10,000	217.92	217.70	
20,000	213.42	213.95	
30,000	209.97	209.61	
40,000	204.58	204.24	
50,000	200.21	200.52	0.6269
60,000	195.89	195.47	
70,000	191.61	192.67	
80,000	187.38	189.12	
90,000	183.15	183.20	

Each well exhibited some variability in its predicted flow rates. These differences can be attributed to the trajectory of the production wells connected to the single manifold. Well A was drilled more vertically than the others, resulting in relatively higher productivity. The differing trajectories lead to slight variations in production performance.

Figure 18 and Table 8 consolidate the flow rates for all three wells, showing the combined simulated and estimated flow rates. The total flow rate starts near 218 MMSCF/D and decreases to 183 MMSCF/D. The strong alignment between the simulated and predicted values across all wells highlights the model's overall accuracy and its potential applicability for predicting total production in complex gas fields.

3.2. Flow Rate and Bottomhole Pressure Trends

The model successfully identified and predicted the natural decline in flow rates associated with reservoir depletion over time. Figure 19 illustrates the predicted flow rate trends for Wells A, B, and C. For Well A, the flow rate decreased from an initial value of 72.57 MMSCF/D to approximately 58.67 MMSCF/D over the course of the study. This trend aligns with the typical behavior observed in gas wells for which sustained production leads to gradual declines in flow rates due to pressure depletion.

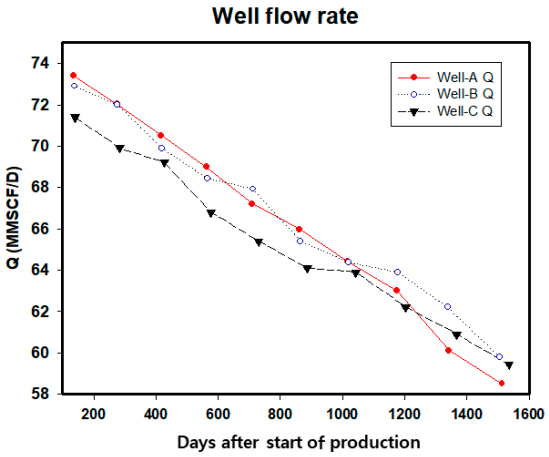

Figure 19. Estimated flow rate trends of each well changes over time.

Variations in production behavior across Wells B and C were also notable, with flow rate trends reflecting differences in reservoir pressure and initial production conditions. These insights are critical for operators, as understanding these trends allows for better long-term planning and resource management.

In addition to flow rates, the model provided accurate forecasts of BHP, which are essential for assessing reservoir health and operational efficiency. Figure 20 demonstrates the BHP trends for each well throughout the production period. For Well A, the BHP

declined from 5149 psi to 4147 psi, highlighting the effects of continued gas extraction on reservoir pressure dynamics.

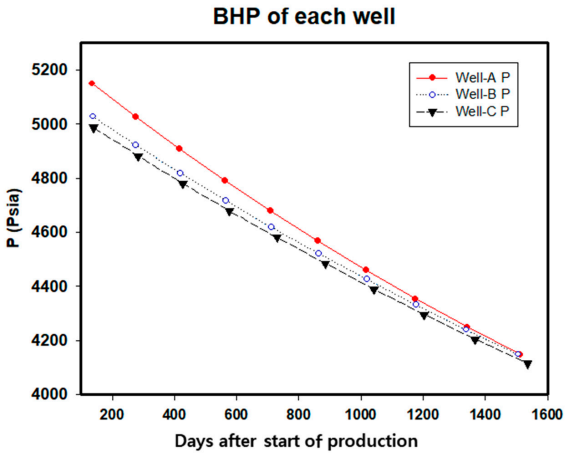

Figure 20. Estimated bottomhole pressure (BHP) trends of each well change over time.

The steady decline in BHP observed across the wells indicates a uniform depletion pattern, reinforcing the need for careful pressure management to prevent issues such as gas locking or equipment failure. Effective monitoring of BHP is crucial for maintaining safe operational conditions, and the model's accuracy in predicting these values enhances its applicability for operational decision-making.

Future research could focus on incorporating dynamic parameters, such as changes in fluid composition and temperature variations, to further improve the model's accuracy. Additionally, applying the model to more complex reservoir systems, including those with multi-phase flows or significant heterogeneity, will enhance its generalizability and applicability across diverse gas field operations.

3.3. Implications, Limitations, and Future Work

The machine-learning-based approach developed in this study shows great promise for optimizing production forecasting and enhancing real-time decision-making in gas field operations. By utilizing field data such as flow rates, BHP, THP, WGR, and OGR, the model can quickly detect unexpected flow and issue alarms during steady-state production, improving both operational efficiency and predictive maintenance.

However, the model has certain limitations. It may not fully capture the complexities of flow dynamics, particularly under multiphase flow or highly heterogeneous reservoir conditions. The differences between our model's results and those from PIPESIM stem from the inherent limitations of the machine learning approach, as do PIPESIM's nonlinear characteristics. However, the overall impact of these differences remains minimal.

Future research should focus on incorporating dynamic parameters such as fluid composition and temperature variations to enhance the model's accuracy in handling evolving reservoir conditions. Expanding the model to account for multiphase flow and applying it to unconventional or deepwater reservoirs will further broaden its practical utility. Additionally, validating the model with real-time production data is essential to ensure its robustness in real-world applications.

4. Conclusions

Efficient production management is key to maximizing profits and minimizing operational costs in gas field operations. This includes the proactive detection of maintenance needs and potential risks in operating gas fields. The aim of this study was to develop a production prediction solution capable of responding to various issues in real time. To this end, we tested data from three gas wells scheduled for production to predict changes in production rates and BHP. A deep learning-integrated model was proposed to estimate pro-

duction flow rates for each well, utilizing the initial pressure and the expected cumulative gas production profile. The analysis yielded the following conclusions:

(1) When comparing the results of the commercial software with the deep learning model, the minimum, maximum, and average error rates of the total flow rate were 0.04%, 2.35%, and 1.5%, respectively. This indicates that the model's predictions closely matched actual values.
(2) As production progressed, different production profiles emerged based on the gas field's IPR. This demonstrates the necessity of adjusting the top-side pressure during production to properly distribute the flow rate and achieve optimal production.
(3) The findings of this study are expected to assist in the optimal allocation of production rates in future gas field operations. Using production data and BHP profiles under normal operating conditions, any real-time deviations beyond a certain threshold can be flagged as danger signals, allowing for immediate response. This can be utilized for stable plant operations and predictive maintenance of facilities, while also improving workforce efficiency in areas currently reliant on manual labor.
(4) To achieve more accurate analyses, it is essential to address limitations such as the availability of diverse training data and potential overfitting issues in certain machine learning models. Increasing the volume of training data, carefully selecting AI models, and cross-validating multiple models will significantly improve predictive performance.

In addition to providing a highly accurate machine learning model for production forecasting, this study offers practical insights into optimizing gas field management. The proposed model can be integrated into existing DOF infrastructures, enhancing real-time decision-making and operational efficiency. By reducing reliance on costly commercial software and enabling autonomous analysis, this approach has the potential to lower operational costs and improve the longevity of gas field infrastructure.

Author Contributions: Conceptualization, Y.L.; methodology, Y.L.; software, J.H.; validation, Y.L. and J.H.; formal analysis, S.H.; investigation, J.H.; resources, Y.L.; data curation, J.H.; writing—original draft preparation, J.H.; writing—review and editing, S.H.; visualization, J.H.; supervision, S.H.; project administration, Y.L.; funding acquisition, S.H. and Y.L. All authors have read and agreed to the published version of the manuscript.

Funding: This work was supported by the National Research Foundation of Korea (NRF) grant funded by the Korea government (MSIT) (No. RS-2023-00210272, RS-2024-00410397).

Data Availability Statement: Data are contained within the article.

Conflicts of Interest: The authors declare no conflicts of interest.

References

1. Energy Institute. Natural Gas Consumption Worldwide from 1998 to 2023 (In Billion Cubic Meters). Available online: https://www.statista.com/statistics/282717/global-natural-gas-consumption/ (accessed on 30 September 2024).
2. Li, Q.; Li, Q.; Han, Y. A Numerical Investigation on Kick Control with the Displacement Kill Method during a Well Test in a Deep-Water Gas Reservoir: A Case Study. *Processes* **2024**, *12*, 2090. [CrossRef]
3. Li, Q.; Li, Q.; Wang, F.; Wu, J.; Wang, Y. The Carrying Behavior of Water-Based Fracturing Fluid in Shale Reservoir Fractures and Molecular Dynamics of Sand-Carrying Mechanism. *Processes* **2024**, *12*, 2051. [CrossRef]
4. Markeset, T.; Moreno-Trejo, J.; Kumar, R. Maintenance of subsea petroleum production systems: A case study. *J. Qual. Maint. Eng.* **2013**, *19*, 128–143. [CrossRef]
5. Moreno-Trejo, J.; Markeset, T. *Identifying Challenges in the Maintenance of Subsea Petroleum Production Systems*; Springer: Berlin/Heidelberg, Germany, 2012; pp. 251–259.
6. Abdalla, R. *Transforming the Industry: Digitalization and Automation in Oil and Gas Wells*; IntechOpen: London, UK, 2023.
7. Bahari, M.; Arpaci, I.; Der, O.; Akkoyun, F.; Ercetin, A. Driving Agricultural Transformation: Unraveling Key Factors Shaping IoT Adoption in Smart Farming with Empirical Insights. *Sustainability* **2024**, *16*, 2129. [CrossRef]
8. Zeba, G.; Dabić, M.; Čičak, M.; Daim, T.; Yalcin, H. Technology mining: Artificial intelligence in manufacturing. *Technol. Forecast. Soc. Change* **2021**, *171*, 120971. [CrossRef]

9. Tariq, Z.; Aljawad, M.S.; Hasan, A.; Murtaza, M.; Mohammed, E.; El-Husseiny, A.; Alarifi, S.A.; Mahmoud, M.; Abdulraheem, A. A systematic review of data science and machine learning applications to the oil and gas industry. *J. Pet. Explor. Prod. Technol.* **2021**, *11*, 4339–4374. [CrossRef]
10. Hussain, M.; Alamri, A.; Zhang, T.; Jamil, I. Application of Artificial Intelligence in the Oil and Gas Industry. In *Engineering Applications of Artificial Intelligence*; Springer: Berlin/Heidelberg, Germany, 2024; pp. 341–373.
11. MarketsandMarkets Digital Oilfield Market by Processes (Reservoir, Production, Drilling Optimizations, Safety-, Asset Management), Technology (loT, Al, Robotics & Automation, Big Data & Analytics, Cloud Computing), Solution, Application, Region—Global Forecast to 2029; 2024. Available online: https://www.marketsandmarkets.com/Market-Reports/digital-oilfield-market-904.html (accessed on 19 September 2024).
12. Suslick, S.B.; Schiozer, D.; Rodriguez, M.R. Uncertainty and risk analysis in petroleum exploration and production. *Terrae* **2009**, *6*, 30–41.
13. Elharith, M.; Huey, H.Y.; Tewari, R.D.; Claire, L.; Fawzi, N.S.M.; Schulze-Riegert, R. Integrated modeling of a complex oil rim development scenario under subsurface uncertainty. *J. Pet. Explor. Prod. Technol.* **2019**, *9*, 2417–2428. [CrossRef]
14. Qiu, K.; Fan, K.; Chen, X.; Lei, G.; Wei, S.; Navik, R.; Li, J. A new approach for production prediction in onshore and offshore tight oil reservoir. *J. Mar. Sci. Eng.* **2023**, *11*, 2079. [CrossRef]
15. Nikitin, N.O.; Revin, I.; Hvatov, A.; Vychuzhanin, P.; Kalyuzhnaya, A.V. Hybrid and automated machine learning approaches for oil fields development: The case study of Volve field, North Sea. *Comput. Geosci.* **2022**, *161*, 105061. [CrossRef]
16. Rabczuk, T.; Bathe, K.-J. *Machine Learning in Modeling and Simulation*; Springer: Cham, Switzerland, 2023; Volume 10, pp. 149–178.
17. Li, H.; Tan, Q.; Deng, J.; Dong, B.; Li, B.; Guo, J.; Zhang, S.; Bai, W. A Comprehensive Prediction Method for Pore Pressure in Abnormally High-Pressure Blocks Based on Machine Learning. *Processes* **2023**, *11*, 2603. [CrossRef]
18. Adegboye, M.A.; Fung, W.-K.; Karnik, A. Recent advances in pipeline monitoring and oil leakage detection technologies: Principles and approaches. *Sensors* **2019**, *19*, 2548. [CrossRef] [PubMed]
19. Rostamian, A.; de Sousa Miranda, M.V.; Mirzaei-Paiaman, A.; Botechia, V.E.; Schiozer, D.J. Analysis of different objective functions in petroleum field development optimization. *J. Pet. Explor. Prod. Technol.* **2024**, 1–21. [CrossRef]
20. Adeboye, Y.; Ubani, C.; Oribayo, O. Prediction of reservoir performance in multi-well systems using modified hyperbolic model. *J. Pet. Explor. Prod. Technol.* **2011**, *1*, 81–87. [CrossRef]
21. Baruah, B.; Kalita, P.; Pandey, L.; Tiwari, P. Petroleum Reservoirs and Oil Production Mechanisms. In *Microbial Enhanced Oil Recovery: Principles and Potential*; Springer: Singapore, 2022; pp. 1–21.
22. Economides, M.J. *Petroleum Production Systems*; Pearson Education: Bloomington, MN, USA, 2013.
23. Golan, M.; Whitson, C.H. *Well Performance*; Prentice Hall: Upper Saddle River, NJ, USA, 1991.
24. Beggs, H.D. *Production Optimization Using Nodal (TM) Analysis*; Ogci: London, UK, 2003.
25. Ahmed, T. *Reservoir Engineering Handbook*; Gulf Professional Publishing: Houston, TA, USA, 2018.
26. Katz, D.L.V. *Handbook of Natural Gas Engineering*; McGraw-Hill: New York, NY, USA, 1959.
27. King, G. Introduction to petroleum and natural gas engineering. 2018. Available online: https://www.e-education.psu.edu/png301/node/508 (accessed on 19 September 2024).
28. Okotie, S.; Ikporo, B. *Reservoir Engineering*; Springer: Berlin/Heidelberg, Germany, 2019.
29. Mattar, L.; McNeil, R. The "flowing" gas material balance. *J. Can. Pet. Technol.* **1998**, *37*. [CrossRef]
30. Mattar, L.; Anderson, D.; Stotts, G. Dynamic material balance-oil-or gas-in-place without shut-ins. *J. Can. Pet. Technol.* **2006**, *45*. [CrossRef]
31. LeCun, Y.; Bengio, Y.; Hinton, G. Deep learning. *Nature* **2015**, *521*, 436–444. [CrossRef] [PubMed]
32. Goodfellow, I. *Deep Learning*; MIT Press: Cambridge, MA, USA, 2016.
33. Jordan, M.I.; Mitchell, T.M. Machine learning: Trends, perspectives, and prospects. *Science* **2015**, *349*, 255–260. [CrossRef]
34. Abadi, M.; Barham, P.; Chen, J.; Chen, Z.; Davis, A.; Dean, J.; Devin, M.; Ghemawat, S.; Irving, G.; Isard, M. {TensorFlow}: A system for {Large-Scale} machine learning. In Proceedings of the 12th USENIX Symposium on Operating Systems Design and Implementation (OSDI 16), Savannah, GA, USA, 2–4 November 2016; pp. 265–283.
35. Raschka, S.; Julian, D.; Hearty, J. *Python: Deeper Insights into Machine Learning*; Packt Publishing Ltd.: Birmingham, UK, 2016.
36. Guo, B. *Petroleum Production Engineering, a Computer-Assisted Approach*; Elsevier: Amsterdam, The Netherlands, 2011.
37. Brill, J.; Mukherjee, H. Multiphase Flow in Wells. *Soc. Pet. Eng.* **1999**, *39*, 15–21. [CrossRef]
38. Wiggins, M.L. Inflow and outflow performance. In *Society of Petroleum Engineers*; OnePetro: Richardson, TX, USA, 2007. [CrossRef]
39. Hansen, L.S.; Pedersen, S.; Durdevic, P. Multi-phase flow metering in offshore oil and gas transportation pipelines: Trends and perspectives. *Sensors* **2019**, *19*, 2184. [CrossRef] [PubMed]